Impacts of climate or vegetation changes on evapotranspiration and streamflow trends in a large water-limited basins?

Qiang Liu[1,2], Zhifeng Yang[1,2], Liqiao Liang[3], Nan Wang[1,2]

1 Key Laboratory for Water and Sediment Sciences, Ministry of Education, School of Environment, Beijing Normal University, Beijing 100875, China

2 State Key Laboratory of Water Environment Simulation, School of Environment, Beijing Normal University, Beijing 100875, China

3 Key Laboratory of Tibetan Environment Changes and Land Surface Processes, Institute of Tibetan Plateau Research, Chinese Academy of Sciences, Beijing 100101, China

Abstract:

Hydrological processes regulate interactions between climate, vegetation, and soil, particularly in water-limited regions. Causes behind changes in evapotranspiration (E) and streamflow (Q) in water-limited regions in the Yellow River Basin (YRB), China, were investigated in this study. It was assumed that vegetation type and extent remained fixed and unchanged throughout the study period while the effective rooting depth (Z_e) changed under climate change scenarios. The Budyko framework was used to explore climate change and vegetation impacts on E and Q on static vegetation and dynamic vegetation rooting depths. Both precipitation (P) and potential evapotranspiration (E_p) exhibited negative trends, which resulted in decreasing trends in dynamic Z_e scenarios. Decreasing trends in Z_e in combination with climatic changes altered the partitioning of P into E and Q. For the dynamic scenario, total E and Q were predicted at −1.73% and 28.22%, respectively, greater by comparison to the static scenario. Although climate change regulated changes in E and Q, Z_e response to climate change had a greater overall contribution to changes in hydrological processes. Results from this study indicated that with the exception of vegetation type and extent, changes in Z_e scenarios can also affect the partitioning of P into E and Q, which in itself should help regulate climate change impacts on water resources.

Key words: ecohydrological processes; evapotranspiration; streamflow; effective rooting depth; water-limited basin

1. Introduction

Partitioning of precipitation (P) into evapotranspiraiton (E) and streamflow (Q) on land surfaces reflects a hydrologic response to land use and climate forcing. Given that this phenomenon impacts water availability globally (Xu et al., 2013), understanding such processes is critical to improve water

resource management practices. A large number of studies have previously been conducted to quantify climate or vegetation change impacts on catchment water balances. Evidence shows that changes in climatic conditions that result from P and potential evapotranspiration (E_p), for example, have a sizeable impact on Q (e.g., IPCC, 2007; Oudin et al., 2009; Liang et al., 2013). Additionally, changes in land use type can dramatically alter water balances on different scales, such as the reduction in Q observed in the Loess Plateau, China, that the Grain for Green project (GGP) had identified (McVicar et al., 2010) (GGP is an ecological restoration initiative that was instigated in 1999 by the Chinese Central Government to re-vegetate former farming and grazing land with perennial species). For these reasons, quantifying impacts of climate and vegetation change on Q remains a challenge for hydrological sciences.

Along with complex, physically-based distributed hydrological models (bottom-up approach), simple coupled water and energy balance models (top-down approach), such as the Budyko framework, have attracted considerable attention in recent years (e.g., Zhang et al., 2001; Yang et al., 2007; Brümmer et al., 2012; Donohue et al., 2012). According to the Budyko framework (1974), available water and energy are the primary factors that determine E rates, which also control the partitioning of P into E and Q. Because the original version of the Budyko model only included climatic variables, an adjustable parameter has been incorporated into the model to reflect the influence of watershed characteristics (e.g., Fu et al., 1981; Choudhury, 1999; Zhang et al., 2001; Yang et al., 2007). Even though this watershed characteristics parameter (n) has been investigated by a number of studies (Zhang et al., 2001; Yang et al., 2009; Donohue et al., 2010), its relation to physical attributes remains obscure (Gerrits et al., 2009; Donohue et al., 2012; Liu and McVicar, 2012). Combining equations by Choudhury (1999) and Porporato et al. (2004), Donohue et al. (2012) deduced relationships between n

and ecohydrological processes, such as storm depth (α), the plant-available soil water holding capacity (κ), and the effective rooting depth (Z_e), which offers new insight into understanding the response of hydrological processes to impacts of climate change and vegetation. While numerous studies have investigated impacts of climate and vegetation on hydrological processes (e.g., Liu and McVicar, 2012; Wang and Tang, 2014), few have explored impacts of vegetation on hydrological processes from the point of view of the response of vegetation to climate change. The objectives of this study were: to explore temporal trends in *E* and *Q* and assess the relative contribution of climate and vegetation changes on *E* and *Q* in the Yellow River Basin (YRB), a large water-limited basin in China.

2. Hydrological model and materials

2.1 Hydrological model

This study employed the improved version of the Budyko hydrological model with the addition of an ecohydrological adjustable parameter (*n*) to assess impacts of climate and vegetation changes on *E* and *Q*. By incorporating this adjustment parameter, the Budyko model can be expressed as follows (e.g., Choudhury's equation (1999)):

$$E = \frac{PE_p}{\left(P^n + {E_p}^n\right)^{(1/n)}}, \quad (1)$$

where *n* is a catchment-specific parameter (dimensionless), which reflects the influence of catchment characteristics on the partitioning of *P* between *E* and *Q*. By combining the equation provided by Porporato et al. (2004) and Choudhury (1999), Donohue et al. (2012) used Z_e, mean depth per storm event (α), and the fractional plant-available water holding capacity (κ) to explain *n*.

$$n = 0.21\frac{\kappa Z_e}{\alpha} + 0.60. \quad (3)$$

Ignoring changes in storage, this steady state water balance model can be expressed as follows (Donohue et al., 2011; Roderick and Farquhar, 2011; Liu and McVicar, 2012):

$$Q = P - E = P - \frac{PE_p}{\left(P^n + {E_p}^n\right)^{(1/n)}}. \quad (3)$$

Equations (2) and (3) constitute the Budyko-Choudhury-Porporato model (BCP model).

In order to obtain the ecohydrological parameter (n), κ was set to static state as designated by the Harmonized World Soil Database (version 1.0) (FAO/IIASA/ISIRC/ISS-CAS/JRC, 2008). Due to the lack of basin wide, long-term, sub-daily P data used to calculate α, the variable was estimated using daily P throughout 1961–2010 (Porporato et al., 2004). Given that Z_e is comparatively unobservable on a catchment scale (Gao et al., 2014), it was calculated for YRB by applying the Z_e model by Guswa (2008) for large water-limited basins. The vegetation fraction for trees and grass was calculated by means of the Normalized Difference Vegetation Index (NDVI), and this was obtained from the NASA Ames Ecological Forecasting Lab website (http://ecocast.arc.nasa.gov/data/pub/gimms/3g/), which was used to calculate Z_e. The fraction of vegetation was also used to reflect the extent of vegetation within the entire basin.

2.2 Materials

YRB is approximately 5400 km long with a basin drainage area of 7.95×10^5 km^2 (Fig. 1). Its headwaters originate in the Tibetan Plateau, flowing through the Loess Plateau and the North China Plain before finally emptying into the Bohai Sea. Since most of the river flows through arid and semiarid regions, increased agricultural and industrial water usage in combination with decreases in P has led to overall decreases in Q (Liu et al., 2008; McVicar et al., 2002; Nakayama, 2011). Data from the National Climate Center of the China Meteorological Administration (CMA) were used to investigate impacts of climate change on water resources at 89 meteorological stations. Monthly E_p was calculated from monthly wind speed, daylight hours, relative humidity, and average air temperature using the Penman equation (Shuttle worth 1993). NDVI data were obtained from the

Global Land Cover Facility (http://www.glcf.umd.edu/) and were used to calculate the fraction of photosynthetically active radiation (PAR) absorbed by vegetation (f_{PAR}).

For this study, it was assumed that vegetation type and extent were fixed and remained unchanged throughout the study period (1961– 2010) while Z_e changed under the dynamic influence of climatic change. Two scenarios were generated for this study in accordance to the BCP model. For the static Z_e scenario, 1961 Z_e was fixed for the 1961– 2010 simulation period. For the dynamic Z_e scenario, Z_e was influenced by specific water and energy conditions of each grid cell in accordance with specific changes in climatic conditions.

(Fig. 1)

3. Results

3.1 Changes in ecohydrological processes

YRB P and E_p temporal trends (1961–2010) are provided in Fig. 2. On a basin scale, the average slope for P was −0.96 mm a^{-2} with a range between −2.37 mm a^{-2} and 1.03 mm a^{-2} (Fig. 2a) while the average slope for E_p was −0.13 mm a^{-2} with a range between −3.38 and1.47 mm a^{-2} (Fig. 2b). E_p/P exhibited increasing trends with an average increase of 0.004 mm a^{-2} (Fig. 2).

According to conclusions that stated that the higher the P (or lower E_p/P) the deeper the Z_e (Schenk and Jackson, 2002; Donohue et al., 2012), Z_e was calculated for YRB, a large water-limited basin in China (data provided in Fig. 3). Average static Z_e (Fig. 3a) (1961 was used to set the base condition of Z_e) ranged between 89 and 2245 mm (with an average of 381 mm) while average dynamic Z_e throughout 1961–2010 ranged between 82 and 1818 mm. Dynamic Z_e was influenced by decreasing P trends, resulting in an insignificant decreasing trend with a slope of −0.12 mm a^{-2}.

(Fig. 3)

4.2 Changes in streamflow and evapotranspiration

(Fig. 4)

126 Modeled *E* time series using the BCP model incorporating dynamic *n* (average *n* was 1.81 on a basin
127 scale) are provided in Fig. 4. Results showed similar trends to observed *E* (calculated using *P*−*Q*).
128 Furthermore, the Nash–Sutcliffe model efficiency coefficient (*NSE*) reached up to 0.85 for the dynamic
129 Z_e scenario while NSE was 0.83 for the static Z_e scenario. On account of overestimations of high *E* (i.e.,
130 during years 1961 and 1964) and the underestimation of high *E* (i.e., 2002), modeled *E* under the
131 dynamic Z_e scenario exhibited a negative trend (−0.81 mm a^{-2}) and was thus in opposition to
132 observations (0.23 mm a^{-2}). Modeled *E* under the static Z_e scenario also exhibited a negative trend with
133 a slope of −0.78 mm a^{-2}.

134 (Fig. 5)

135 Relative differences in modeled annual total *Q* and *E* between static Z_e and dynamic Z_e scenarios are
136 provided in Fig. 5. Results showed that: (*i*) For the dynamic Z_e scenario (Fig. 4a), total *E* was predicted
137 to be 1.73% less than the static Z_e scenario while, conversely, total *Q* (Fig. 4b) was predicted to be
138 28.22% greater than the static Z_e scenario; and (*ii*) decreasing trends were detected in most areas of the
139 basin for *E* while increasing trends were detected in most areas of the basin for *Q*.

140 **4.3 Relative contribution of climatic and vegetation changes on *E* and *Q***

141 Temporal trends in *E* calculated from both static and dynamic Z_e scenarios are respectively provided in
142 Fig. 6a and b. Results showed that: (*i*) Temporal trends for both static and dynamic Z_e scenarios
143 exhibited similar spatial patterns, i.e., most areas of the basin contributed to negative (decreasing) *E*
144 trends and only the northwestern region contributed to positive (increasing) *E* trends; (*ii*) temporal
145 trends in *E* under the static Z_e scenario ranged between −2.70 and 1.41 mm a^{-2} with an average increase
146 of −0.81 mm a^{-2} (Fig. 6a) while temporal trends in *E* under the dynamic Z_e scenario ranged between
147 −2.86 and 1.41 mm a^{-2} with an average increase of −0.80 mm a^{-2} (Fig. 6b); and (*iii*) significant trends

($P < 0.05$) in E under static (Fig. 6c) and dynamic (Fig. 6d) Z_e scenarios showed similar patterns for YRB while the extent of these increasing trends per area were significant under the static Z_e scenario (Fig. 6d).

(Fig. 6)

(Fig. 7)

The relative contribution of climate and vegetation (Fig. 7a and 7b) were calculated for each grid cell. Results showed that climate regulated temporal trends in E while changes in Z_e only contributed slightly to changes in E. Using the differential of E or Q to variables (e.g., $\partial E/\partial P$) multiplied by changes in variables (e.g., dP), contributions of different variables can be obtained ($\partial E/\partial P * dP$). For example, following Donohue et al. (2012), the "typical variability" observed for each variable between 1961 and 2010 was determined (represented by the standard deviation of annual values). Results showed that: (*i*) Changes in P caused the greatest variability in E (or Q), generally followed by variability in Z_e, α, and E_p; (*ii*) changes in P contributed greater to changes in E (when compared to Q); and (*iii*) summed contributions of climatic variables (P, E_p, and α) to E and Q were greater than Z_e, especially for E.

(Table 1)

5. Discussion

As demonstrated by this study (Fig. 1), both P and E_p showed decreasing trends while E_p/P showed a slight increasing trend (0.004 mm a^{-2}) throughout 1961–2010. Results were consistent with those reported by Liu and McVicar (2012). Decreasing trends in P (with an average trend of −0.96 mm a^{-2}) or increasing trends in E_p/P resulted in decreasing trends in Z_e (data provided in Fig. 2). Strong interactions are known to exist between climate, vegetation, and soil properties that subsequently result

in specific hydrologic partitioning on a catchment scale (Troch et al., 2013). Inevitably, it is available water (P) and energy (represented by E_p) that regulate vegetation patterns. Degradation in vegetation caused by decreasing P has been previously reported in YRB (e.g., Xin et al., 2008). In particular, changes in vegetation extent and type (mainly resulting from human activity) are major causes of Q change (Li et al. 2007; Liu et al., 2009). For example, changes in vegetation patterns prompted by land use changes (e.g., such as those determined by the Grain for Green project in the Loess Plateau) inevitably alter hydrological processes and result in a decrease in Q (McVicar et al. 2007; Cao et al., 2011). On the one hand, numerous studies have concluded that vegetation change was the main cause for changes in hydrological processes, such as observed changes in Q in the Yiluo River basin (Liu et al., 2009). On the other hand, other studies reported that climate variability in certain regions have had a greater influence on surface hydrology than land use changes, such as that observed in the Heihe River basin, China (Li et al., 2009), as well as the upper Mississippi River basin (Frans et al., 2013) .

In combination with climate change, this study explored how vegetation impacts hydrological processes from an alternative aspect, i.e., assessing Z_e response to climate change and its impacts on Q and E. According to the Budyko framework, the greater the P the deeper the rooting depth (Schenk and Jackson, 2002).Furthermore, modeled E under dynamic and static Z_e scenarios exhibited negative trends while observed E exhibited positive trends (Fig. 3). Vegetation structure profoundly regulates the annual surface hydrological cycle and is a cause and consequence of surface water balances (Gentine et al., 2012). For this study, following Donohue et al. (2012), Z_e in combination with α and κ were used to calculate n (1.81 average). Results were similar to n (n = 1.76) calculated from a nonlinear fitted model by Liu and McVicar (2012). Given the scarcity of Z_e data, validation of modeled Z_e is difficult to obtain for larger basins (Donohue et al., 2012). From the n calculated for each grid cell, it was shown that

simulated E and Q fitted well with observed values (data provided in Fig. 3). Z_e alteration contributed greater to changes in Q and E (Fig. 4 and Table 1), which indicated that the response of vegetation to climatic change can alter the partition of P into E and Q. The BCP model with the addition of ecohydrological parameters (such as Z_e, α, and κ) captured effects of watershed characteristics on partitioning of P into E and Q. Results can also reflect relative contributions (provided in Fig. 5 and Fig. 6). For example, Fig. 5c and Fig. 5d show that significant temporal trends in E yielded different results between static and dynamic Z_e scenarios. Fig. 6 shows that climate change regulates temporal trend changes in E, which is consistent with data provided in Table 1. Furthermore, given that soil, topography, vegetation, and climate are intrinsically interconnected, Gentine et al. (2012) attempted to use the Budyko curve to explain ecohydrological controls of soil water balances. Further research should focus more attention on mechanisms of watershed parameters and improve accuracy of the Budyko framework as it relates to different temporal and spatial scales.

5. Conclusions

Climate change and vegetation impacts on Q and E can be explored using the BCP model with the addition of adjustable ecohydrological parameters (such as Z_e, α, and κ). According to the "typical variability" of different variables, climate change and vegetation impacts were obtained for the static and dynamic Z_e scenarios investigated for this study. The following conclusions can be drawn from this study:

(i) The BCP model in combination with simulated static and dynamic Z_e scenarios captured effects of changes in climate and vegetation on E or Q. In this study, simulated E under static and dynamic Z_e scenarios exhibited negative trends with an average increase of −0.78 and −0.81 mm a^{-2}, respectively. For the dynamic scenario, total E and Q were respectively predicted to be −1.73% and 28.22% greater

than the static scenario, which exhibited obvious spatial variation.

(*ii*) As predicted, although climate change regulates changes in E and Q, Z_e response to climate change contributed greater to changes in E and Q in the water-limited region investigated. Results indicated that with the exception of vegetation type and extent, Z_e scenarios were able to alter the partitioning of P into E and Q. These results should help our understanding of interactions between climate, vegetation, and hydrological processes, and help to regulate water resources over basin scales.

Acknowledgement:

This study was supported by the National Science Foundation for Innovative Research Group (no. 51121003), the Fundamental Research Funds for the Central Universities (no. 2012LYB12), and the Beijing Higher Education Young Elite Teacher Project (no. YETP0259). We would like to thank the National Meteorological Information Center, the China Meteorological Administration, and the Yellow River Conservancy Commission for providing meteorological and streamflow data.

References:

Allen, R.G., L.S. Pereira, D. Raes, and M. Smith (1988), Crop evapotranspiration: Guidelines for computing crop water requirement. *FAO Irrig. and Drain.* Paper No.56. FAO: Rome, Italy.

Bonan, G.B. (2001), Observational evidence for reduction of daily maximum temperature by croplands in the Midwest United States, *J. Climate*, 14, 2430–2442.

Brümmer, C., T.A. Black, R.S. Jassal , N.J. Grant, D.L. Spittlehouse, B. Chen, Z. Nesic, B.D. Amiro, M.A. Arain, A.G. Barr, C.P.A. Bourque, C. Coursolle, A.L. Dunn, L.B. Flannagan, E.R. Humphreys, P.M. Lafleur, H.A. Margolis, J.H. McCaughey, and S.C. Wofsy (2012), How climate

and vegetation type influence evapotranspiration and water use efficiency in Canadian forest, peatland and grassland ecosystems, *Agr. Forest Meteorol.*, 153, 14–30.

Budyko, M. I. (1974), Climate and Life, *Acad. Pr.*, 508 pp.

Cao, S.X., L. Chen, D. Shankman, C. Wang, X. Wang, and H. Zhang (2011), Excessive reliance on afforestation in China's arid and semi-arid regions: Lessons in ecological restoration, *Earth-Sci. Rev.*, 104, 240–245.

Choudhury, B.J. (1999), Evaluation of an empirical equation for annual evaporation using field observations and results from a biophysical model, *J. Hydrol.*, 216, 99–110.

Donohue, R.J., M.L. Roderick, and T.R. McVicar (2010), Can dynamic vegetation information improve the accuracy of Budyko's hydrological model? *J. Hydrol.*, 390 (1-2), 23–34.

Donohue, R.J., M.L. Roderick, and T.R. McVicar (2011), Assessing the differences in sensitivities of runoff to changes in climatic conditions across a large basin, *J. Hydrol.*, 406, 234–244.

Donohue, R.J., M.L. Roderick, and T.R. McVicar (2012), Roots, storms and soil pores: incorporating key ecohydrological processes into Budyko's hydrological model, *J. Hydrol.*, 436–437, 35–50.

Frans, C., E. Istanbulluoglu, V. Mishra, F. Munoz-Arriola, and D.P. Lettenmaier (2013), Are climatic or land cover changes the dominant cause of runoff trends in the Upper Mississippi River Basin? *Geophys. Res. Lett.*, 40, 1104–1110, doi:10.1002/grl.50262.

Fu, B.P. (1981), On the calculation of the evaporation from land surface (in Chinese), *Scientia. Atmosp.Sinica*, 5, 23–31.

Gentine, P., P. D'Odorico, B.R. Lintner, G. Sivandran, and G. Salvucci (2012), Interdependence of climate, soil, and vegetation as constrained by the Budyko curve, *Geophys. Res. Lett.*, 39, L19404, doi: 10.1029/2012GL053492.

Gerrits, A.M.J., H.H.G. Savenije, E.J.M. Veling, and L.P. Fister (2009), Analytical derivation of the Budyko curve based on rainfall characteristics and a simple evaporation model, *Water Resour. Res.*, 45, W04403, doi:10.1029/2008WR007308.

IPCC (2007), Climate Change 2007: The Physical Science Basis. Contribution of Working Group I to the Fourth Assessment, *Camb. U. Pr.*, New York.

Li, L.J., L. Zhang, H. Wang, J. Wang, J.W. Yang, D.J. Jiang, J.Y. Li, and D.Y. Qin (2007), Assessing the impact of climate variability and human activities on streamflow from the Wuding River basin in China, *Hydrol. Processes.*, 21, 3485–3491.

Li, Z., W.Z. Liu, X.C. Zhang, and F.L. Zheng (2009), Impacts of land use change and climate variability on hydrology in an agricultural catchment on the Loess Plateau of China, *J. Hydrol.*, 377, 35–42.

Liang, L.Q., and Q. Liu **(**2013), Streamflow sensitivity analysis to climate change for a large water-limited basin, *Hydrol. Processes*, doi: 10.1002/hyp.9720.

Liu, Q., and T.M. McVicar (2012), Assessing climate change induced modification of Penman potential evaporation and runoff sensitivity in a large water-limited basin, *J. Hydrol.*, 464–465, 352–262.

Liu, Q., and Z.F. Yang (2010), Quantitative estimation of the impact of climate change on actual evapotranspiration in the Yellow River Basin, China, *J. Hydrol.*, 395, 226–234.

Liu, Q., Z.F. Yang, and B.S. Cui (2008), Spatial and temporal variability of annual precipitation during 1961-2006 in Yellow River Basin, China, *J. Hydrol.*, 361, 330–338.

Liu, Q., Z.F. Yang, B.S. Cui, T. Sun (2009), Temporal trends of Hydro-climatic variables and runoff response to climatic variability and vegetation changes in the Yiluo River basin, China, *Hydrol. Processes.*, 23(21), 3030–3039.

McVicar, T.R., L.T. Li, T.G. Van Niel, L. Zhang, R. Li, Q.K. Yang, X.P. Zhang, X.M. Mu, Z.M.Wen, W.Z. Liu, Y.A. Zhao, Z.H. Liu, and P. Gao (2007a), Developing a decision support tool for China's re-vegetation program: Simulating regional impacts of afforestation on average annual streamflow in the Loess Plateau, *Forest Ecol. and Manag.*, 251 (1–2), 65–81.

McVicar, T.R., G.L. Zhang, A.S. Bradford, H.X. Wang, W.R. Dawes, L. Zhang, and L.T. Li (2002), Monitoring regional agricultural water use efficiency for Hebei Province on the North China Plain, *Aust. J. Agr. Res.*, 53, 55–76.

McVicar, T.R., T.G. Van Niel, L.T. Li, Z.M. Wen, Q.K. Yang, R. Li, F. Jiao (2010), Parsimoniously modelling perennial vegetation suitability and identifying priority areas to support China's re-vegetation program in the Loess Plateau:Matching model complexity to data availability, *Forest Ecol Manag.*, 259 (7), 1277–1290.

Nakayama, T. (2011), Simulation of the effect of irrigation on the hydrologic cycle in the highly cultivated Yellow River Basin, *Agr. Forest Meteorol.*, 151, 314–327.

Oudin, L., V. Andreassian, J. Lerat, and C. Michel (2008), Has land cover a significant impact on mean annual streamflow? An international assessment using 1508 catchments, *J. Hydrol.*, 357 (3–4), 303–316.

Porporato, A., E. Daly, and I. Rodriguez-Iturbe (2004), Soil water balance and ecosystem response to climate change, *Am. Nat.*,164 (5), 625–632.

Roderick, M.L., and G.D. Farquhar (2011), A simple framework for relating variations in runoff to variations in climatic conditions and catchment properties, *Water Resour. Res.*, 47, W00G07, doi:10.1029/2010WR009826.

Schenk, H.J., and R.B. Jackson (2002), Rooting depths, lateral root spreads and

below-ground/above-ground allometries of plants in water-limited ecosystems, *J. Ecol*., 90, 480–494.

Shuttleworth, W.J. (1993), Evaporation. In: D.R. Maidment (Editor), *Handbook Hydrol.*, McGraw-Hill, Sydney.

Troch, P.A., G. Garrllo, M. Sivapalan, T. Wagener, and K. Sawicz (2013), Climate-vegetation-soil interactions and long-term hydrologic partitioning: signatures of catchment co-evolution, *Hydrol. Earth Syst. Sc.*, 10, 2927–2954.

Xin, Z.B., J.X. Xu, and Z. Wei (2008), Spatiotemporal variations of vegetation cover on the Chinese Loess Plateau (1981–2006): Impacts of climate changes and human activities, *Sci China Ser. D: Earth Sc*, 51, 67–78.

Xu, X.L., W. Liu, B.R. Scanlon, L. Zhang, and M. Pan (2013), Local and global factors controlling water-energy balances within the Budyko framework, *Geophys. Res. Lett.*, 40, 6123–6129.

Yang, D.W., F.B. Sun, Z.Y. Liu, Z.T. Cong, G.H. Ni, and Z.D. Lei(2007), Analyzing spatial and temporal variability of annual water-energy balance in non-humid regions of China using the Budyko hypothesis, *Water Resour. Res.*, 43, W04426, http://dx.doi.org/10.1029/2006WR005224.

Yang, D.W., W.W. Shao, P.J.F. Yeh, H.B. Yang, S. Kanae, and T. Oki (2009), Impact of vegetation coverage on regional water balance in the non-humid regions of China, *Water Resour. Res.*, 45, W00A14, doi:10.1029/2008WR006948.

Yang, H., D. Yang, Z. Lei, and F. Sun (2008), New analytical derivation of the mean annual water balance equation, *Water Resour. Res.*, 44, W03410, doi:10.1029/2007WR006135.Zhang, L., W.R. Dawes, and G.R. Walker (2001), The response of mean annual evapotranspiration to vegetation changes at catchment scale, *Water Resour. Res.*, 37 (3), 701–708

Gao, H., Hrachowitz, M., Schymanski, S.J., Fenicia, F., Sriwongsitanon, N., Savenije, H.H.G., 2014. Climate controls how ecosystems size the root zone storage capacity atcatchment scale, *Geophys. Res. Lett.*, DOI: 10.1002/2014GL061668.

FAO/IIASA/ISIRC/ISS-CAS/JRC, 2008.Harmonized World Soil Database (version 1.0) FAO, Rome, Italy and IIASA, Laxenburg, Australia.

Wang, D.B., Y, Tang (2014). A one-parameter Budyko model for water balance captures emergent behavior in darwinianhydrologic models, *Geophys. Res. Lett.*, 41, 4569-4577.

Table and Figure captions:

Table 1 Summaries of E and Q sensitivity to changes in ecohydrological conditions throughout the study period (1961–2010). Shown for each variable and zone are E and Q sensitivity coefficients, observed variability per variable, and typical variability in E caused by driving variables. dZ_e is the difference between tree and grass Z_e modeled for the basin.

Fig. 1 Location of the Yellow River.

Fig. 2 Temporal trends in P (a) and E_p (b) (mm a^{-2}) for the Yellow River basin.

Fig. 3 Static Z_e (1961) (a) and average dynamic Z_e (b) (1961–2010) for the Yellow River basin.

Fig. 4 Observed and modeled annual E for the Yellow River basin.

Fig. 5 Modeled percentage differences in mean annual total E (a) and Q (b**)** between static Z_e (Z_e determined for 1961 was fixed throughout the 1961–2010 simulation period) and dynamic Z_e (Z_e was influenced by specific water and energy conditions for each grid cell in accordance with specific climate change conditions). $E_{change} = \left({}^{(E_d - E_s)}/_{E_d}\right) \times 100\%$, where E_{change} is the percentage difference in mean annual total E, and E_d, and E_s are mean annual total E between static Z_e and dynamic Z_e project. $Q_{change} = \left({}^{(Q_d - Q_s)}/_{Q_d}\right) \times 100\%$, where Q_{change} is the percentage difference in mean annual total Q, and Q_d and Q_s are mean annual total E between static Z_e and dynamic Z_e scenarios.

Fig. 6 Temporal trends in E under static Z_e (Fig. 5a) and dynamic Z_e (Fig. 5b) scenarios, and regions exhibiting significant E slopes ($p < 0.05$) for static Z_e (Fig. 5c) and dynamic Z_e (Fig. 5d) scenarios as determined by the Mann–Kendall method.

Fig. 7 Relative contributions of climate (a) and vegetation (b) to changes in E for YRB (areas void of significant trends are showed in white). Relative contributions can be expressed as: $E_c = (S_{sz} / S_{dy}) \times 100\%$, $E_v = ((S_{dz}–S_{sz}) / S_{dz}) \times 100\%$, where E_c is the relative contribution resulting from climate on E; E_v is the relative contribution resulting from vegetation on E; and S_{sz} and S_{dz} are trends ($p < 0.05$) of modeled E under static Z_e and dynamic scenarios, respectively.

Table 1 Summaries of E (left) and Q (right) sensitivity to changes in ecohydrological conditions throughout the study period (1961–2010). Shown for each variable and zone are E and Q sensitivity coefficients, observed variability per variable, and typical variability in E caused by driving variables. dZ_e is the difference between tree and grass Z_e modeled for the basin.

Sensitivity for E	unit	YRB	Sensitivity for Q	unit	YRB
$\partial E/\partial P$	mm a^{-1}/ mm a^{-1}	0.73	$\partial Q/\partial P$	mm a^{-1}/ mm a^{-1}	0.17
dP	mm a^{-1}	59	dP	mm a^{-1}	59
$\partial E/\partial P*dP$	mm a^{-1}	41.9	$\partial Q/\partial P*dP$	mm a^{-1}	10.1
$\partial E/\partial E_p$	mm a^{-1}/ mm a^{-1}	0.05	$\partial Q/\partial E_p$	mm a^{-1}/ mm a^{-1}	−0.05
dE_p	mm a^{-1}	42	dE_p	mm a^{-1}	42
$\partial E/\partial_{Ep}*dE_p$	mm a^{-1}	2.1	$\partial Q/\partial_{Ep}*dE_p$	mm a^{-1}	−2.1
$\partial E/\partial\alpha$	mm a^{-1}/ mm	−10.6	$\partial Q/\partial\alpha$	mm a^{-1}/ mm	10.6
$d\alpha$	mm	0.39	$d\alpha$	mm	0.39
$\partial E/\partial\alpha*d\alpha$ (	mm a^{-1}	−4.2	$\partial Q/\partial\alpha*d\alpha$	mm a^{-1}	4.2
$\partial E/\partial Z_e$	mm a^{-1}/ mm	0.17	$\partial Q/\partial Z_e$	mm a^{-1}/ mm	−0.17
dZ_e	mm	30	dZ_e	mm	30
$\partial E/\partial Z_e$ $*dZ_e$	mm a^{-1}	5	$\partial Q/\partial Z_e$ $*dZ_e$	mm a^{-1}	−5

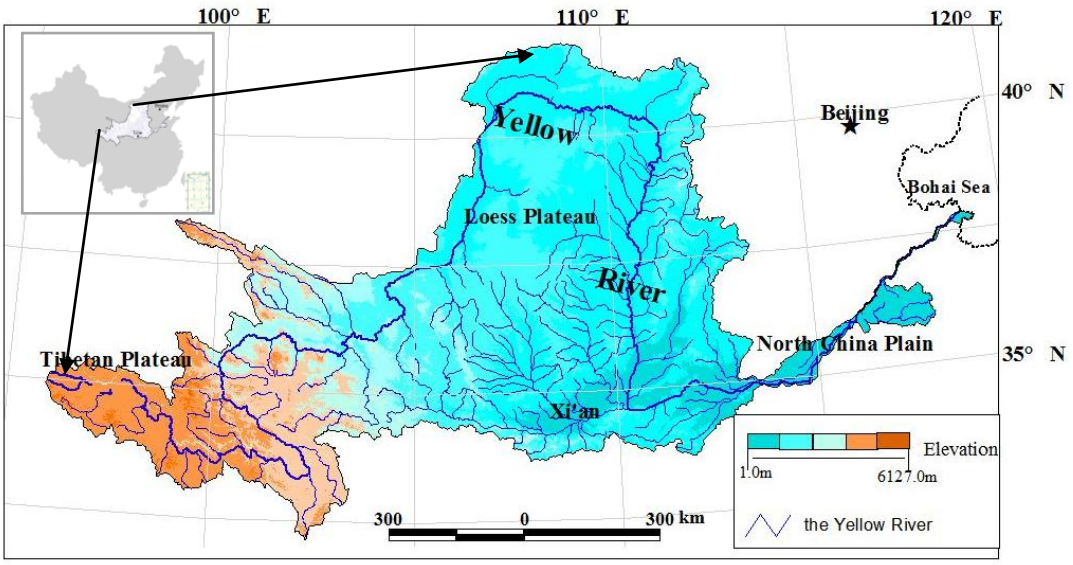

373

374 Fig. 1 Location of Yellow River.

375

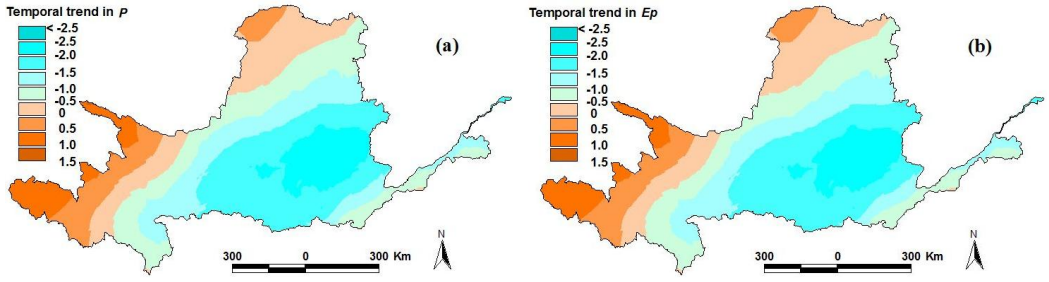

376

377 Fig. 2 Temporal trends in P (a) and E_p (b) (mm a^{-2}) for the Yellow River basin.

378

379

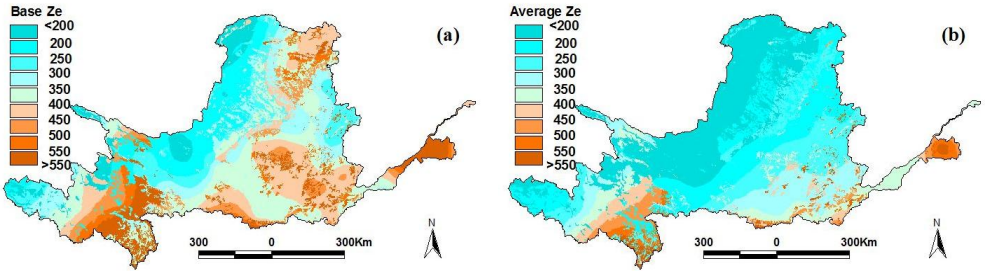

Fig. 3 Static Z_e (1961) (a) and average dynamic Z_e (b) (1961–2010) for the Yellow River basin.

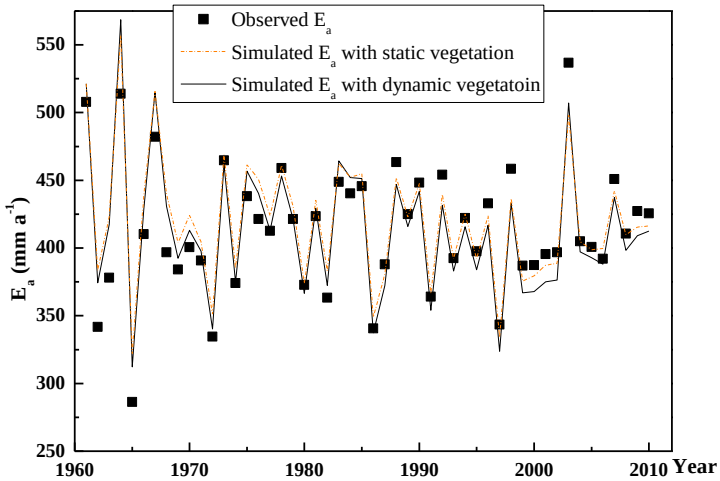

384

385 Fig. 4 Observed and modeled annual *E* for the Yellow River basin.

386

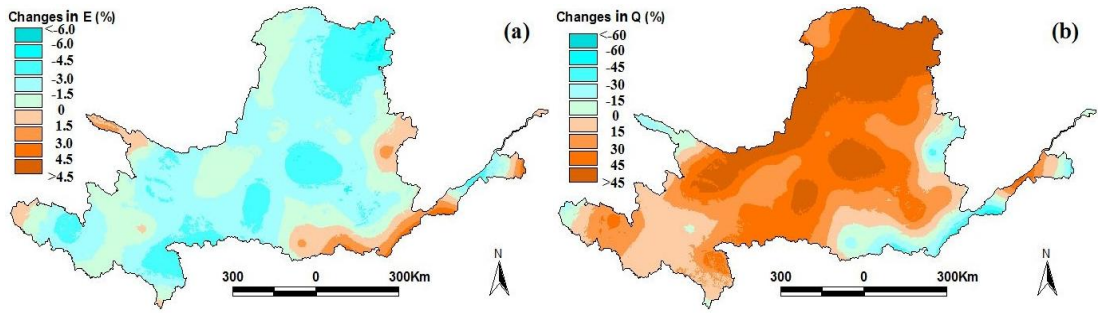

Fig. 5 Modeled percentage differences in mean annual total E (a) and Q (b**)** between static Z_e (Z_e determined for 1961 was fixed throughout the 1961–2010 simulation period) and dynamic Z_e (Z_e was influenced by specific water and energy conditions for each grid cell in accordance with specific climate change conditions). $E_{change} = \left({}^{(E_d - E_s)}/_{E_d}\right) \times 100\%$, where E_{change} is the percentage difference in mean annual total E, and E_d, and E_s are mean annual total E between static Z_e and dynamic Z_e scenarios. $Q_{change} = \left({}^{(Q_d - Q_s)}/_{Q_d}\right) \times 100\%$, where Q_{change} is the percentage difference in mean annual total Q, and Q_d and Q_s are mean annual total E between static Z_e and dynamic Z_e scenarios.

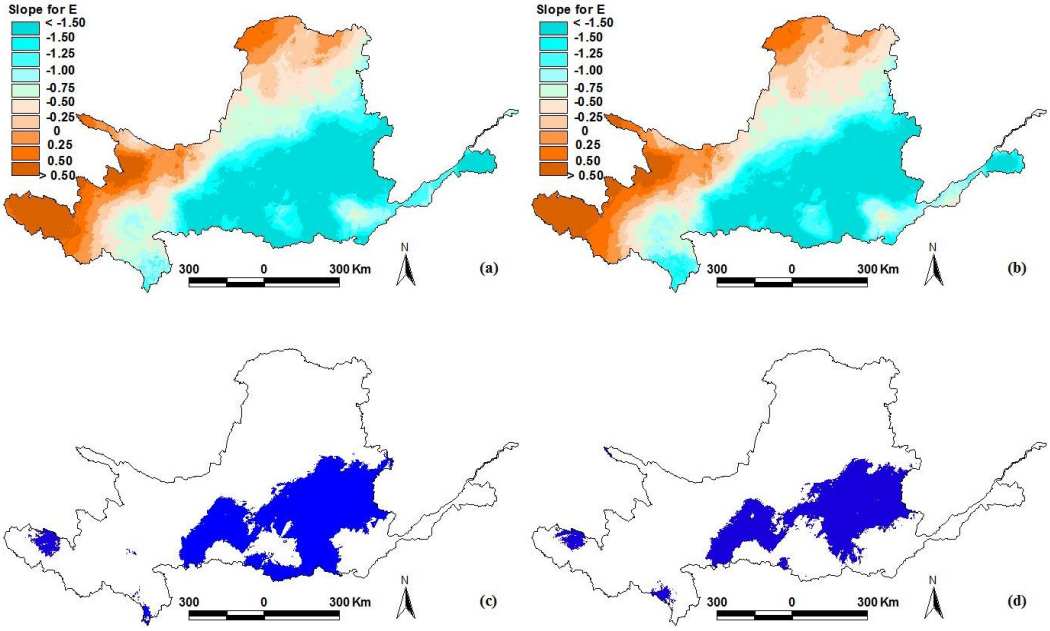

Fig. 6 Temporal trends in E under static Z_e (Fig. 5a) and dynamic Z_e (Fig. 5b) scenarios, and regions exhibiting significant E slopes ($p < 0.05$) for static Z_e (Fig. 5c) and dynamic Z_e (Fig. 5d) scenarios as determined by the Mann–Kendall method.

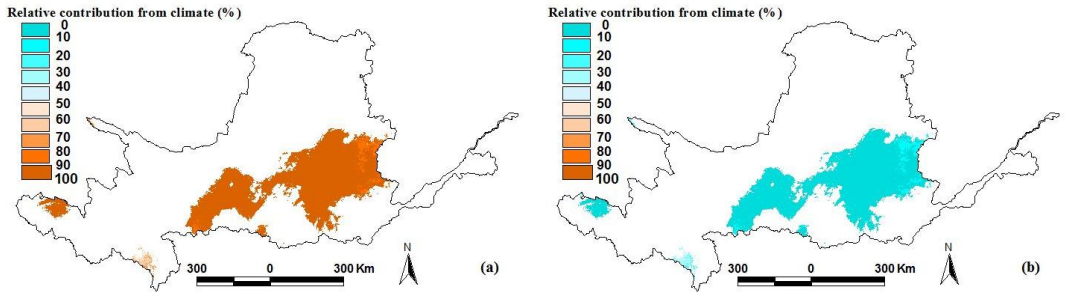

403

404 Fig. 7

405 Relative contributions of climate (a) and vegetation (b) to changes in *E* for YRB (areas void of

406 significant trends are showed in white). Relative contributions can be expressed as:

407 $E_c = (S_{sz} / S_{dy}) \times 100\%$, $E_v = ((S_{dz}–S_{sz}) / S_{dz}) \times 100\%$, where E_c is the relative contribution resulting from

408 climate on *E*; E_v is the relative contribution resulting from vegetation on *E*; and S_{sz} and S_{dz} are trends (p

409 < 0.05) of modeled *E* under static Z_e and dynamic scenarios, respectively.